Journal of Applied Physics

Energetics of native defects in $ZnRh_2O_4$ spinel from hybrid density functional calculations

Cite as: J. Appl. Phys. **125**, 165703 (2019); https://doi.org/10.1063/1.5086799
Submitted: 23 December 2018 . Accepted: 09 April 2019 . Published Online: 24 April 2019

Kodchakorn Simalaotao, Pakpoom Reunchan, Naoto Umezawa, Jiraroj T-Thienprasert, and Adisak Boonchun

Journal of Applied Physics ARTICLE scitation.org/journal/jap

Energetics of native defects in $ZnRh_2O_4$ spinel from hybrid density functional calculations

Cite as: J. Appl. Phys. **125**, 165703 (2019); doi: 10.1063/1.5086799
Submitted: 23 December 2018 · Accepted: 9 April 2019 ·
Published Online: 24 April 2019

Kodchakorn Simalaotao,[1] Pakpoom Reunchan,[1,2,a)] Naoto Umezawa,[3] Jiraroj T-Thienprasert,[1,2] and Adisak Boonchun[1,2,a)]

AFFILIATIONS

[1]Department of Physics, Faculty of Science, Kasetsart University, Bangkok 10900, Thailand
[2]Thailand Center of Excellence in Physics (ThEP Center), Commission on Higher Education, Bangkok 10400, Thailand
[3]Semiconductor R&D Center, Samsung Electronics, Hwaseong-si, Gyeonggi-do 18448, Republic of Korea

[a)]**Authors to whom correspondence should be addressed:** fsciasb@ku.ac.th and pakpoom.r@ku.ac.th

ABSTRACT

Most transparent conducting oxides (TCOs) exhibit *n*-type conductivity and are difficult to dope into *p*-type. Therefore, the development of efficient *p*-type TCOs is challenging. $ZnRh_2O_4$ spinel has been recognized as a potential *p*-type TCOs. However, the source of its *p*-type conductivity has not been elucidated. In this study, we used hybrid density functional calculations to investigate the energetics and electronic properties of native defects in $ZnRh_2O_4$, including vacancies, interstitials, and cation antisites. We found that all acceptor-type defects including Zn vacancies, Zn antisites, and Rh vacancies acted as deep centers. Charge neutrality analysis suggested that undoped $ZnRh_2O_4$ may behave as a *p*-type semiconductor with hole concentrations of 10^{18}–10^{19} cm^{-3} under the extreme O-rich/Rh-poor growth condition in which ZnRh has a low formation energy and acts as the major source of hole carriers. However, under realistic growth conditions, the experimentally determined hole concentration significantly exceeds that which is calculated. Our results suggest that native point defects are unlikely to be responsible for the high hole concentrations observed in $ZnRh_2O_4$ spinel.

I. INTRODUCTION

Display technology materials must provide a combination of high electrical conductivity and optical transparency.[1–3] Transparent conducting oxides (TCOs) are well known and widely used in liquid crystal displays, touch screens, solar cells, plasma and organic light emitting (OLED) displays, and smart windows.[4–7] Most commercially available TCOs are *n*-type semiconductors.[8–11] The development of efficient *p*-type TCOs for transparent electronic devices is thus challenging. One way to form a *p*-type TCO is by introducing metal *d* states in oxygen 2*p* levels of the valence state. Kawazoe *et al.*[12] proposed this mechanism to achieve *p*-type TCO behavior in $CuAlO_2$ and later extended this technique to other Cu-based TCOs. This type of band engineering can be extended to the investigation of Zn d^6 spinels such as $ZnRh_2O_4$, $ZnCo_2O_4$, and $ZnIr_2O_4$ as alternative *p*-type TCOs. Spinel oxides with partially occupied *d* orbitals (non-d^0 and non-d^{10}) such as Rh^{3+} have recently attracted interest as potential *p*-type TCOs. Transparency among these materials originates from splitting of Rh^{3+} 4*d* orbitals due to ligand field splitting when the Rh cation is in octahedral coordination with oxygen atoms.[13,16] The bandgap consists of the gap between the fully occupied t_{2g}^6 and empty e_g^0 levels. Mizoguchi *et al.*[14] reported that thin film $ZnRh_2O_4$ spinel is a *p*-type semiconductor with a bandgap of ~2.1 eV. Later, Dekkers *et al.*[15] reported *p*-type conductivity in polycrystalline thin film $ZnRh_2O_4$ and a higher bandgap of 2.74 eV. The activation energy associated with conductivity was observed, and cation vacancies were tentatively suggested as sources of hole carriers. A more recent study by Mansourian-Hadavi *et al.*[16] reported a bandgap of 2.2 eV and the transport properties of crystalline $ZnRh_2O_4$. Their high-temperature electrical property analysis indicated activated mobility and thus small polaron conduction.[16] However, small polaron stability and the *p*-type $ZnRh_2O_4$ conduction mechanism remain under debate.[17]

A number of theoretical calculations have been reported that follow the aforementioned experimental studies. Scanlon and Watson[18] calculated the bandgaps of a series of $ZnM_2^{III}O_4$ (M^{III} = Co, Rh, Ir) spinels based on a screened hybrid functional proposed by Heyd *et al.* (HSE06)[19] and showed that $ZnRh_2O_4$ has an indirect bandgap of 2.87 eV. Volnianska and Boguslawski[20] studied native

point defects and *p*-type conductivity in $ZnRh_2O_4$ using the generalized gradient approximation (GGA) + *U* with the +*U* term applied to the Zn 3*d*, Rh 4*d*, and O 2*p* orbitals, i.e., *U*(Zn) = *U*(Rh) = *U*(O) = 4 eV. Based on their calculated formation energies, both Zn vacancies (V_{Zn}) and Zn antisites (Zn_{Rh}) were reported to be shallow acceptors. This finding nearly mirrored their GGA results. Later, the same authors again studied native point defects in $ZnRh_2O_4$ via GGA + *U*, but with different *U* parameters, i.e., *U*(Rh) = *U*(O) = 5 eV and *U*(Zn) = 0. With this *U* parameter, both V_{Zn} and Zn_{Rh} defects were determined to be shallow acceptors. However, their calculated formation energies indicated thermodynamic transition levels (−/0) at ∼0.35 and ∼0.40 eV, and thus suggested that V_{Zn} and Zn_{Rh} are deep acceptors.[21] The inconsistent results for these two acceptors lead one to wonder what value of *U* should be adopted to give reasonable defect electronic structure and energetics results. Thus, GGA + *U* should be applied to defect calculations with caution. As discussed in previous work by Alkauskas *et al.*,[22–24] the charge transition levels of defects with atomically localized states (deep defect level) obtained via semilocal and hybrid density functionals are almost identical when the energy scales are aligned using an external quantity such as the vacuum level. On the other hand, shallow defect levels with only delocalized wave functions are rigidly shifted in line with the band edges that they pertain to upon bandgap opening. Deviation from the ideal alignment of the transition level of the intermediate case is related to the extent of the defect wave function and is intrinsically system dependent. Based on the semilocal functional (GGA), it is still possible to describe defect charge transition levels and formation energies properly once the valence and conduction band edges of the host materials are correctly positioned with respect to the vacuum level. These can be compared to experimentally determined ionization energies and electron affinities.

Recently, Amini *et al.*[25] performed a new investigation of the source of *p*-type conductivity in $ZnM^{III}_2O_4$ (M^{III} = Co, Rh, Ir) spinels using the HSE06 functional. Based on the calculated formation energies, both V_{Zn} and Zn_{Rh} were reported as shallow acceptors. Thus, the researchers concluded that the *p*-type conductivity observed in $ZnRh_2O_4$ originates from V_{Zn} and Zn_{Rh}. Although the HSE06 functional used in this work has been proven to appropriately describe semiconductor defect electronic and structural properties, the method used for ionic relaxations does not guarantee convergence of interatomic forces. Instead of residual interatomic forces, transition level position differences were used as convergence criteria. This nonstandard method might produce unexpected ionic relaxations of some defects. In fact, the nearest neighbor atoms of the TiO_2,[26] MgO,[27] and ZnO[28] cation vacancies were found to relax outward while those of the $ZnRh_2O_4$ cation vacancies were reported to relax inward.[25] In addition, although their calculations used a 96-atom supercell, corrections due to finite cell size effects for charged defects were not mentioned in their report.

In this paper, we perform density functional theory (DFT) calculations using the HSE06 hybrid functional to investigate the energetic and structural/electrical properties of native point defects in $ZnRh_2O_4$ spinel. This includes vacancies, interstitials, and cation antisites. Our calculations use the most advanced technique currently available for comprehensive studies of point defects.[29] Native defect stabilities are compared using formation energies calculated under representative growth conditions. Our findings are summarized as follows. (i) All acceptor-type defects, i.e., V_{Zn}, Rh vacancies (V_{Rh}), and Zn_{Rh} act as deep centers, are unlikely to be ionized, and would not give rise to hole carriers at room temperature. (ii) Based on charge neutrality analysis, native point defects are unlikely to lead to high *p*-type conductivity in $ZnRh_2O_4$ under any equilibrium growth conditions. The Fermi level is pinned ∼0.3 eV above the valence band maximum (VBM), resulting in a hole concentration of $\sim 10^{18}\,cm^{-3}$ even under extreme growth conditions in which acceptor-type defect formation dominates.

II. METHODOLOGY

Our calculations are based on DFT with the HSE06 hybrid functional[19] and the projector augmented wave (PAW) method,[30] as implemented in the Vienna *ab initio* Simulation Package (VASP) code.[31] We used a plane wave basis set with an energy cutoff of 400 eV. The standard Hartree–Fock mixing parameter in the HSE06 approach of 25% was employed, where it yielded a bandgap of 2.89 eV. The Zn ($4s^2\ 3d^{10}$), Rh ($5s^1\ 4d^8$), and O ($2s^2\ 2p^6$) electrons were treated as valence electrons. Our native defect calculations employed a 56-atom supercell. Test calculations were performed using a 224-atom supercell to ensure supercell size convergence in the cases of V_{Zn} and Zn_{Rh}. The difference between the formation energies calculated using the 56-atom and 224-atom supercells was less than 0.1 eV. A set of 2 × 2 × 2 Monkhorst–Pack special *k*-point grids was used for the Brillouin zone integrations. All atoms were relaxed until the residual forces are lower than 0.02 eV/Å. The effects of spin polarization were included for all charge states. The crystal structure and charge density are illustrated using VESTA visualization software.[32]

The formation energy of a defect *D* in the charge state *q* was defined via

$$E_f(D^q) = E_{tot}(D^q) - E_{tot}(ZnRh_2O_4) - \sum_i n_i\mu_i + q(\varepsilon_F + E_V) + E_{corr}, \quad (1)$$

where $E_{tot}(D^q)$ is the total energy of a supercell with defect *D* in charge state *q*. $E_{tot}(ZnRh_2O_4)$ is the total energy of the same supercell without a defect and n_i is the number of atoms of species *i* (Zn, Rh, or O) that have been added to ($n_i > 0$) or removed from ($n_i < 0$) the supercell. The atom that is removed from or added to the supercell is placed in or taken from the reservoir with energy μ_i. The Fermi energy (ε_F) is the energy of the electron reservoir, referenced to the valence band maximum (VBM) E_V. E_{corr} is a sum of relevant correction terms. In our case, it corrected for electrostatic interactions between periodic images of charged defects. The elastic interaction correction was considered but found to be negligible in our case. Undesired interactions between a charged defect with its images in neighboring cells and the homogeneous background charge were corrected using the scheme proposed by Freysoldt *et al.*[33] Here, the dielectric constant of 12.67 obtained via the PBE (Perdew-Burke-Ernzerhof) calculation was used in the correction as it was computationally inexpensive. Since the dielectric constants obtained from PBE and HSE calculations were quite similar as shown using TiO_2,[34] we expected the use of the PBE dielectric constant to yield a similar correction.

Here, we reference chemical potentials $\tilde{\mu}_i$ using the energy per atom of the isolated elemental phase: $\tilde{\mu}_O = \mu_O - \frac{1}{2}E_{tot}[O_2]$, $\tilde{\mu}_{Zn} = \mu_{Zn} - E_{tot}[Zn_{bulk}]$, and $\tilde{\mu}_{Rh} = \mu_{Rh} - E_{tot}[Rh_{bulk}]$. The chemical potentials $\tilde{\mu}_i$ (i = Zn, Rh, O) are treated as variables and can be properly chosen to represent the experimental growth conditions. During equilibrium growth of the $ZnRh_2O_4$ crystal, the chemical potentials $\tilde{\mu}_{Zn}$, $\tilde{\mu}_{Rh}$, and $\tilde{\mu}_O$ which are taken with respect to the total energy per atom of metallic Zn(hcp), metallic Rh(fcc), and molecular O_2 molecule. They are required to satisfy the stability condition $\tilde{\mu}_{Zn} + 2\tilde{\mu}_{Rh} + 4\tilde{\mu}_O = \Delta H_f(ZnRh_2O_4)$, where $\Delta H_f(ZnRh_2O_4)$ is the enthalpy of formation of $ZnRh_2O_4$. Our calculated $H_f(ZnRh_2O_4)$ of −8.44 eV is in reasonable agreement with the experimental value of −7.89 eV.[35] Indeed, the upper limit of each atomic chemical potential is set to zero to avoid the formation of metallic Zn, metallic Rh, and gaseous O_2.

The following constraints are enforced to avoid precipitation of the unwanted compounds ZnO, RhO_2, and Rh_2O_3:

$$\tilde{\mu}_{Zn} + \tilde{\mu}_O < \tilde{\mu}_{ZnO}, \tag{2}$$

$$\tilde{\mu}_{Rh} + 2\tilde{\mu}_O < \tilde{\mu}_{RhO_2}, \tag{3}$$

$$2\tilde{\mu}_{Rh} + 3\tilde{\mu}_O < \tilde{\mu}_{Rh_2O_3}. \tag{4}$$

These constraints defined a domain in a two-dimensional chemical potential coordinate system with $\tilde{\mu}_{Zn}$ and $\tilde{\mu}_{Rh}$ axes (shaded area in Fig. 1). In order to maintain equilibrium growth of $ZnRh_2O_4$, $\tilde{\mu}_{Zn}$ and $\tilde{\mu}_{Rh}$ are allowed to vary only within the domain and $\tilde{\mu}_O$ is determined only by the equilibrium condition mentioned above.

The thermodynamic transition level $\varepsilon_D(q/q')$ is given by the Fermi-level position at which the formation energy of a defect in charge q [$E_f(D^q)$] is equal to the formation energy of the same defect in charge q' [$E_f(D^{q'})$].

$$\varepsilon_D(q/q') = \frac{E_f(D^q; \varepsilon_F = 0) - E_f(D^{q'}; \varepsilon_F = 0)}{q' - q}, \tag{5}$$

where $E_f(D^q;\varepsilon_F = 0)$ is the formation energy of D^q taken at $\varepsilon_F = 0$. This defines the kinks in the formation of energy plots as functions of the Fermi-level position. Note that ε_F ranges over the bandgap and is referenced to the VBM.

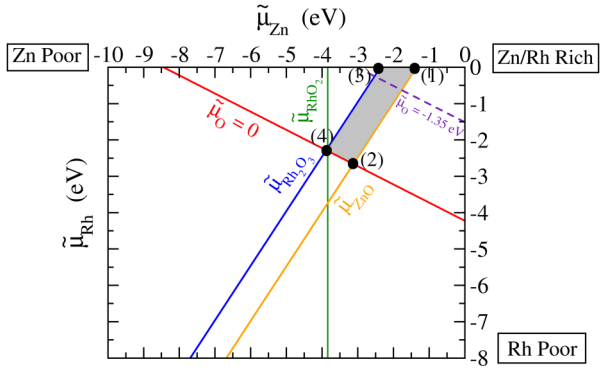

FIG. 1. The thermal equilibrium growth conditions allowed for $ZnRh_2O_4$ (shaded area). The axes are the chemical potentials of $\tilde{\mu}_{Zn}$ and $\tilde{\mu}_{Rh}$, referenced using the energy per atom of its elemental phase. The purple dashed line represents the experimental growth condition that corresponds to an oxygen chemical potential of −1.35 eV.

III. RESULTS AND DISCUSSION

The spinel structure of $ZnRh_2O_4$ can be described by a $Fd\bar{3}m$ space group, which is shown as a 56-atom conventional cell in Fig. 2(a). The $ZnRh_2O_4$ spinel contains a face-centered cubic of oxygen anions with the Zn and Rh cations occupying tetrahedral and octahedral sites, respectively. The calculated local atomic structures of the Zn and Rh atoms are shown in Figs. 2(b) and 2(c), respectively. The Zn atom is tetrahedrally coordinated with four O atoms (with a Zn–O bond length of 2.01 Å and a O–Zn–O bond angle of ∼109.5°). The Rh atoms bond with O atoms via distorted octahedral coordination (two sets of O–Rh–O bonds with angles ∼84.6° and 95.4° and one set of 2.04 Å Rh–O bonds). For the oxygen local structure, each O atom forms asymmetric tetrahedral bonds with its neighboring three Rh atoms and one Zn atom [Fig. 2(d)]. These three Rh–O bonds are equivalent with bond lengths of 2.04 Å, while the Zn–O bond length is 2.01 Å. Our calculated lattice constant, energy bandgap, and enthalpy of formation are in good agreement with previously calculated and experimental values, as shown in Table I.

Figure 3 shows the calculated band structure and projected densities of states (PDOS) of $ZnRh_2O_4$ spinel. We find that $ZnRh_2O_4$ has an indirect bandgap; the valence band maximum (VBM) is located at the X point in the Brillouin zone and the conduction band minimum (CBM) is located near X along the Γ-X direction. Our calculated indirect bandgap is 2.89 eV, which is in good agreement with the value previously calculated using HSE06 of 2.87 eV[25] as well as the experimental value of 2.74 eV.[15] Note that experimentally determined bandgaps vary from 2.10 to 2.74 eV.[14] From the PDOS shown in Fig. 3(b), it is clear that both the VBM and CBM are formed primarily of 4d-Rh orbitals. This is consistent with the electronic structure reported in Refs. 17 and 18. The VBM is nearly dispersionless (a flatband), which indicates a heavy hole-effective mass. The 3d-Zn peak observed experimentally via X-ray photoemission spectroscopy is reported to appear −9.2 eV below the VBM.[15] Previous HSE calculations predicted that this peak would appear −7.8 eV below the VBM,[18] which is in line with the value of −7.7 eV observed in this work [Fig. 3(b)].

In order to investigate the energetics of native defects in $ZnRh_2O_4$, we selected four different sets of chemical potential values that correspond to points (1), (2), (3), and (4) in Fig. 1. The selected sets of chemical potentials ($\tilde{\mu}_{Zn}$, $\tilde{\mu}_{Rh}$, $\tilde{\mu}_O$) are given in Table II. Points (1) and (3) correspond to the lowest possible value of μ_O, which indicates O-poor growth conditions. Points (2) and (4) correspond to the highest possible value of μ_O, which indicates O-rich growth conditions. Points (1) and (3) also correspond to Zn/Rh-rich and Rh-rich growth conditions, respectively,

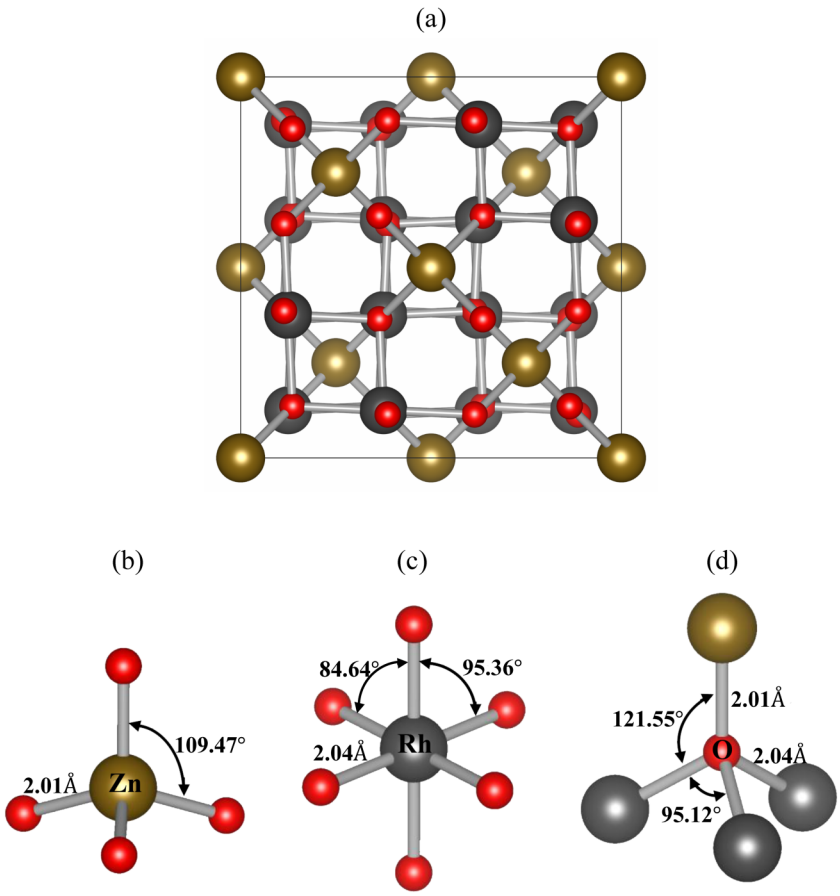

FIG. 2. (a) An illustration of the 56-atom $ZnRh_2O_4$ conventional cell and the local atomic structures of its (b) Zn, (c) Rh, and (d) O atoms. The calculated equilibrium Zn–O and Rh–O bond lengths and angles are also listed. Gold, gray, and red atoms represent Zn, Rh, and O, respectively.

while points (2) and (4) correspond to Rh-poor and Zn-poor growth conditions, respectively.

The calculated formation energies of native defects including V_{Zn}, V_{Rh}, O vacancies (V_O), Zn_{Rh}, Rh substituted for Zn (Rh_{Zn}), Rh interstitials (Rh_i), Zn interstitials (Zn_i), and O interstitials (O_i) for the selected growth conditions are shown in Fig. 4. Here, we focus only on isolated native defects and exclude native defect complexes from the present study. The lower and upper Fermi level limits represent the VBM and CBM, respectively. These formation energy plots show only the possible charge states of each defect that yield the minimum formation energy at a given Fermi-level position. The slope of the line thus reflects the most stable charge state of a defect.

Figure 4 shows that cation interstitials (Zn_i and Rh_i) are active donor defects in $ZnRh_2O_4$. The Zn interstitial creates an *s*-like state

TABLE I. Lattice parameter (*a*), energy bandgap (E_g), and enthalpy of formation (ΔH_f) calculated using the HSE functional. Previously calculated and experimental values are also listed.

	$ZnRh_2O_4$		
	Our calculation	Previous work[25]	Exp.[15]
a (Å)	8.51	8.49	8.49
E_g (eV)	2.89	2.91	2.74
ΔH_f (eV)	−8.44	−7.81	−7.89[35]

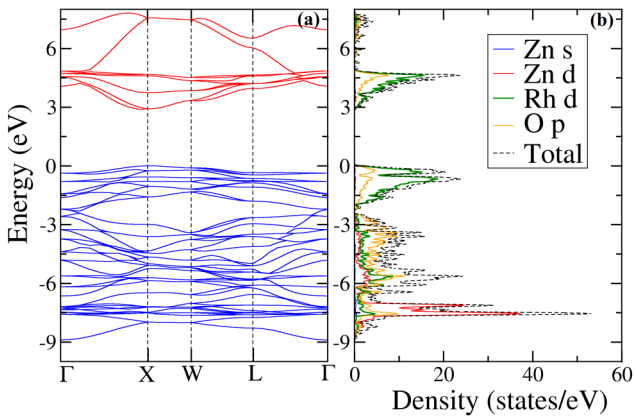

FIG. 3. (a) The band structure and (b) PDOS of $ZnRh_2O_4$ spinel calculated using the HSE06 functional. The valence band maximum is set to zero.

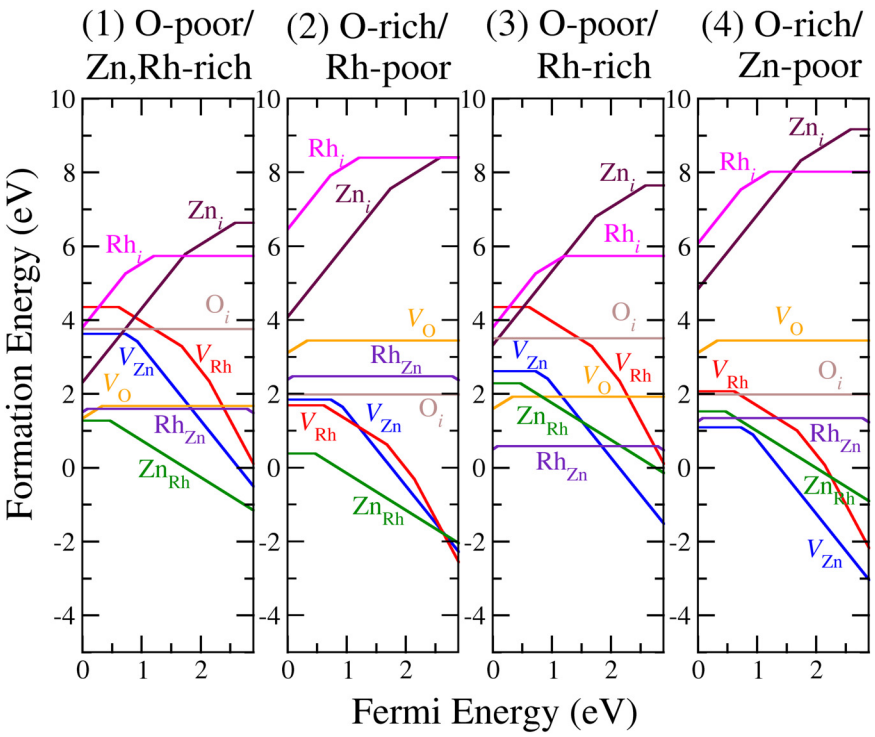

FIG. 4. Formation energies as a function of the Fermi levels (referenced to the valence band maximum) of native defects in $ZnRh_2O_4$ under growth conditions that correspond to points (1), (2), (3), and (4) in Fig. 1.

below the CBM. It is stable in 2+, 1+, and neutral charge states. The thermodynamic transition levels ε(2+/+) and ε(1+/0) are located 1.74 and 2.59 eV above the VBM, respectively, which indicates that it is a deep donor. The Rh interstitial is stable in 2+, 1+, and neutral charge states with the thermodynamic transition levels ε(2+/+) and ε(+/0) 0.73 and 1.21 eV above the VBM, respectively. However, they have high formation energies for all Fermi-level bandgap positions. Zn_i and Rh_i have lower formation energies under Zn-rich/Rh-rich growth [condition (1) in Fig. 4] than under other growth conditions. Their formation energies exceed 2 eV even here, which indicates that their concentrations are negligible. They also have formation energies that are at least 2 eV higher formation energy than dominant acceptor defects in *p*-type material (where the Fermi level is at the VBM) under all selected growth conditions. These cation interstitials are thus unlikely to act as compensating centers for acceptors in *p*-type $ZnRh_2O_4$.

Removal of a Zn atom breaks four Zn–O bonds, leaving four dangling O bonds and two holes in the valence band. In the neutral charge state, these two holes, which are derived mostly from the O 2*p* and Rh 4*d* states, prefer to become localized on different O and Rh atoms next to the vacancy. A hole state associated with V_{Zn} is shown in Fig. 5(a). These hole states are located in the bandgap and can accept two additional electrons, thus making V_{Zn} a double acceptor. The transition levels ε(0/−) and ε(−/2−) are located 0.77 eV and 1.00 eV above the VBM for V_{Zn}, respectively, which indicates that V_{Zn} is a deep acceptor. Since the Rh atom is sixfold coordinated with O atoms and the Zn–O and Rh–O bond lengths are comparable, its removal would produce more energy than that of a Zn atom. This is reflected by the fact that V_{Rh} has a higher formation energy than V_{Zn} under almost all selected growth conditions (Fig. 4). A Rh vacancy also introduces *p*-like states that can accept three additional electrons into the bandgap. The transition levels ε(0/−), ε(−/2−), and ε(2−/3−) are, respectively, 0.61, 1.68, and 2.14 eV above the VBM for V_{Rh}.

Given that the oxidation states of Zn and Rh in $ZnRh_2O_4$ are likely to be 2+ and 3+, respectively, Zn_{Rh} is expected to act as a single acceptor. We find that Zn_{Rh} introduces a hole state localized on Rh and O atoms next to the defect [see Fig. 5(b)]. This hole state is located in the bandgap and can accept one electron, thus making Zn_{Rh} a single acceptor that occurs in charge neutral and singly negative charge states. The transition level ε(0/−) is located 0.47 eV above the VBM, which indicates that Zn_{Rh} is a deep acceptor.

Our calculated thermodynamic transition levels show that all three acceptor-type defects V_{Zn}, V_{Rh}, and Zn_{Rh} act as deep acceptors. They are barely ionized at room temperature. However, the formation energies of Zn_{Rh} and V_{Zn} are quite low under growth conditions (1), (2), and (4) in Fig. 4. This suggests that their

TABLE II. Chemical potentials ($\tilde{\mu}_{Zn}$, $\tilde{\mu}_{Rh}$, and $\tilde{\mu}_O$) at selected equilibrium growth conditions indicated in Fig. 1.

Point	$\tilde{\mu}_{Zn}$	$\tilde{\mu}_{Rh}$	$\tilde{\mu}_O$
(1)	−1.35	0.00	−1.77
(2)	−3.13	−2.66	0.00
(3)	−2.36	0.00	−1.52
(4)	−3.88	−2.28	0.00

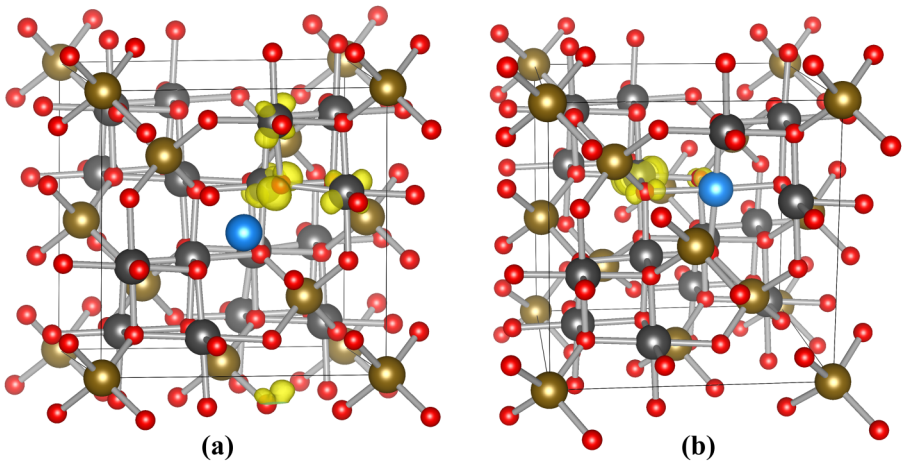

FIG. 5. Charge distributions for hole states of (a) neutral V_{Zn} and (b) Zn_{Rh} in a 56-atom supercell. The blue ball represents the position of V_{Zn} in (a) and the Zn atom in (b). The isosurface level is set to 0.01 electrons $Å^{-3}$ for visualization.

concentrations and associated hole concentrations may be reasonably high. Indeed, high $ZnRh_2O_4$ thin film hole concentrations were indicated experimentally[14,15] and cation vacancies were suggested as a source of hole carriers. In contrast, our analysis (see below) indicates that $\tilde{\mu}_O$ in the experimental growth condition in Ref. 15 is close to the $\tilde{\mu}_O$ that corresponds to O-poor conditions, and thus Zn_{Rh} is likely the dominant acceptor because it has the lowest formation energy among the acceptor defects in *p*-type $ZnRh_2O_4$.

Our suggestion that the antisite Zn_{Rh} is the dominant acceptor in $ZnRh_2O_4$ agrees with the combined experimental and computational studies by Paudel *et al.*[36] and Nagaraja *et al.*,[17] in which Zn_{Rh} was identified as a main source of hole production. $ZnRh_2O_4$ is found to be a "doping Type-II" spinel oxide, which is a *p*-type material with an acceptor level in its bandgap. Moreover, while self-trapped holes were predicted to be stable based on the HSE06 functional,[25] Nagaraja *et al.*[17] predicted them to be unstable in this material based on a DFT + *U* approach. The researchers also predicted that $ZnRh_2O_4$ conductivity is limited by its large effective mass instead of small polaron formation. However, stability and detailed descriptions of native defect–small polaron complexes remain ambiguous and require further investigation.

In addition, our results are qualitatively consistent with the recent HSE06 calculations[25] where Zn_{Rh}, V_{Zn}, and V_{Rh} were found to be single, double, and triple acceptors, respectively. Zn_{Rh} was found to have the lowest formation energy of the three under certain growth conditions. However, Zn_{Rh} and V_{Zn} were reported to be shallow acceptors while our present calculations performed using a similar functional identify them as deep acceptors. This discrepancy may occur for the following reasons: (1) in the present work, the atomic relaxations of the nearest neighbor atom around the defect are different from those reported in Ref. 25 (see Table S1 in the supplementary material). Note that we employed the standard atomic relaxation methodology for defect simulation as described above. (2) The present work adopts a correction due to the finite size of the charged supercell, but none is mentioned in Ref. 25. Our test calculations performed using a 224-atom supercell for V_{Zn} and Zn_{Rh} slightly reduce the thermodynamic transition levels (~0.05 eV for both V_{Zn} and Zn_{Rh}). This indicates that V_{Zn} and Zn_{Rh} remain deep acceptors. In the case of Zn_{Rh}, the value of $\varepsilon(0/-)$ obtained using the 224-atom supercell is located 0.42 eV above the VBM. This is slightly shallower than the value obtained using the 56-atom supercell (~0.47 eV).

Having identified major hole sources and the deep nature of acceptor defects in $ZnRh_2O_4$, our next question is whether native defects are responsible for *p*-type behavior in this material. In order to answer this question, we determined the carrier concentration and pinned Fermi level by satisfying the charge neutrality equation:

$$\sum_i q_i c_i(D^q) + p - n = 0, \tag{6}$$

where the first term is a sum over concentration of all point defects considered in charge state q_i. It should be noted that the results shown in Fig. 6 are based on the assumption that all native defects are immobile at the temperatures of interest and thus fully contribute to the calculated pinned Fermi level and hole concentration via charge neutrality. In practice, some defects can become highly mobile at these temperatures and can be annealed out or passivated by countercharge defects, which makes them electrically inactive.[28,37] Accounting for this may change the calculated pinned Fermi level and hole concentration. However, the mobilities of native defects in $ZnRh_2O_4$ remain unclear. The concentration of a native defect *D* with charge *q* is represented as $c(D^q)$ and related to its formation energy E_f via the below equation:

$$c(D^q) = N_{\text{sites}}/(1 + \exp^{E_f(D^q)/k_B T}), \tag{7}$$

where N_{sites} is the number of possible lattice sites at which the defect can be incorporated per unit volume. A low formation energy defect will result in high concentrations and thus dominates significantly under charge neutrality. Here, we adopt the formation energies obtained from the 56-atom supercell depicted in Fig. 4. The supercell size convergence tests indicate similar results when the formation energies are extrapolated to the dilute limit, that is, *n*

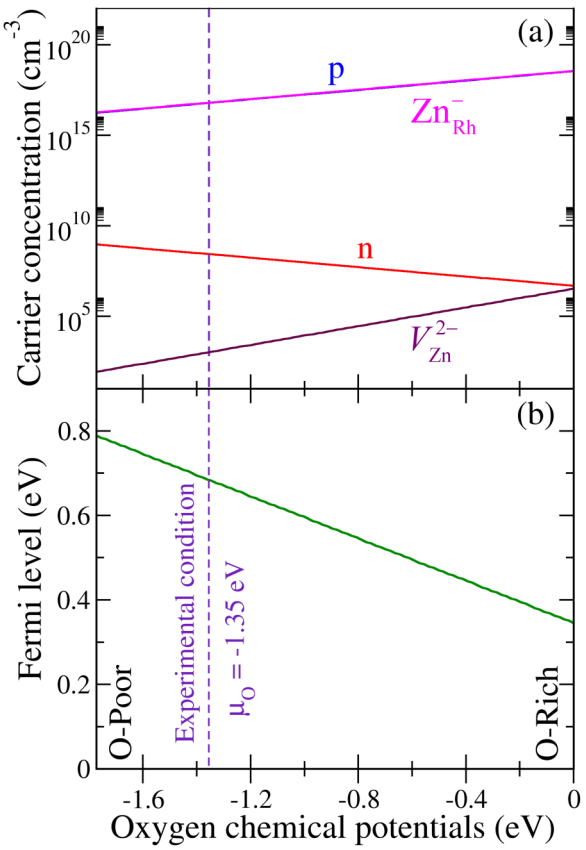

FIG. 6. (a) The defect and carrier concentrations (electrons: *n* and holes: *p*), and (b) pinned Fermi level as functions of the oxygen chemical potential. Note that the two curves in magenta and blue overlap almost completely because the Zn_{Rh}^{-} and hole carrier concentrations are nearly identical. The dashed line indicates the experimental growth condition at the typical annealing temperature of 700 °C and oxygen partial pressure of 0.25 mbar, which correspond to an oxygen chemical potential of −1.35 eV.

is the electron concentration in the conduction band and p is the hole concentration in the valence band as calculated using the Boltzmann approximation. They can be expressed by

$$n = 2\left(\frac{m_e k_B T}{2\pi\hbar^2}\right)^{3/2} \exp^{(\varepsilon_F - E_g)/k_B T}, \tag{8}$$

$$p = 2\left(\frac{m_h k_B T}{2\pi\hbar^2}\right)^{3/2} \exp^{-\varepsilon_F/k_B T}, \tag{9}$$

where m_e and m_h are the electron- and hole-effective masses, respectively, and E_g is the bandgap. The band structure produced via HSE calculations generates an m_h of $1.303m_0$ and m_e of $0.678m_0$. Here, a temperature of 700 °C is used and equilibrium $ZnRh_2O_4$ growth is assumed.[15] In principle, defects with the lowest formation energies dominate governance of charge neutrality. Figure 6 shows the equilibrium carrier concentration and pinned Fermi level as a function of $\tilde{\mu}_O$, which varies from 0 eV (O-rich conditions) to −1.77 eV (O-poor conditions). Here, we represent the results produced when $\tilde{\mu}_O$ varies along the path between points (2) and (1) (Fig. 1) as setting one of the chemical potentials on this path yields the most favorable conditions for Zn_{Rh} formation and thus a *p*-type material. It is clear that the concentration of Zn_{Rh}^{-} is higher than that of V_{Zn}^{2-} and is almost identical to the hole concentration for all values of $\tilde{\mu}_O$. This indicates that Zn_{Rh}^{-} is the dominant acceptor [Fig. 6(a)]. The maximum hole concentration ($\sim 3.5 \times 10^{18}$ cm^{-3}) that produces the lowest Fermi level (~0.35 eV) is reached under O-rich conditions. However, a maximum hole concentration of $\sim 1.4 \times 10^{19}$ cm^{-3} and pinned Fermi level of ~0.31 eV would be obtained if the 975 °C growth temperature used in Ref. 36 were adopted. However, these values were derived under O-rich conditions. O partial pressures under experimental growth conditions could be significantly lower. Thus, the hole concentration should be significantly lower than that estimated above if a realistic chemical potential condition is adopted.

In order to calculate these quantities, we consider an intermediate oxygen chemical potential that corresponds to realistic conditions during $ZnRh_2O_4$ thermal annealing and growth. The oxygen chemical potential is a function of temperature and the oxygen partial pressure as described in Ref. 38,

$$\tilde{\mu}_O(T, p) = \tilde{\mu}_O(T, p_0) + \frac{1}{2} k_B T \ \ln(p/p_0), \tag{10}$$

where $\tilde{\mu}_O(T, p_0)$ is the oxygen chemical potential at the standard pressure $p_0 = 1$ atm, k_B is Boltzmann's constant, and T is the temperature in Kelvin. The growth temperature of 973 K (700 °C) and oxygen partial pressure of 0.25 mbar used in Ref. 15 correspond to $\tilde{\mu}_O = -1.35$ eV, which is represented by the dashed line in Fig. 6. This value of $\tilde{\mu}_O$ yields a hole concentration of $\sim 6.2 \times 10^{16}$ cm^{-3} and pinned Fermi level of ~0.68 eV. A $\tilde{\mu}_O$ of −1.39 eV is obtained when a sintering temperature of 975 °C and the oxygen partial pressure in the air used in Ref. 36 are applied. This yields a hole concentration of $\sim 6.9 \times 10^{17}$ cm^{-3}, far below the value measured in Ref. 17 via the Hall effect of $\sim 1.4 \times 10^{20}$ cm^{-3}. Our analysis suggests that even though native defects can be hole carrier sources under O-rich conditions, they are unlikely to be responsible for the high hole concentration of $\sim 10^{20}$ cm^{-3} observed under realistic experimental conditions. In practice, a variety of active charge defects such as unintentional impurities and complex defects, if formed and energetically stable, can also be charge carrier sources and thus dominate under charge neutrality. If acceptor defect complexes become predominant under experimental growth conditions and are readily ionized, the Fermi level may be pinned closer to the valence band, resulting in a higher hole concentration. This could be a source of the discrepancy between the experimental and theoretical hole concentrations. Hydrogen impurities, which are ubiquitous, and their related complexes are known to play important roles in controlling doping and charge carriers in nitrides[39] and oxides.[40] They are thus expected to participate in controlling $ZnRh_2O_4$ electrical behavior. Computational investigations of the interactions between hydrogen and native defects and their effects on the electronic properties of $ZnRh_2O_4$ are under way.

IV. CONCLUSION

In summary, we have investigated the thermodynamic stabilities and electronic properties of native defects in $ZnRh_2O_4$ using hybrid density functional calculations. We found that all acceptor defects introduced thermodynamic transition levels located above the valence band, indicating their deep nature. The low formation energy of Zn_{Rh} under O-rich/Rh-poor growth conditions indicates that it is likely to be responsible for the *p*-type behavior observed in $ZnRh_2O_4$. However, charge neutrality analysis suggested that hole concentrations of $\sim 10^{18}$–$10^{19}\,cm^{-3}$ are achieved only under O-rich/Rh-poor growth conditions. The intermediate value of the oxygen chemical potential, which represents an experimental growth condition, yielded a hole concentration of $\sim 10^{17}\,cm^{-3}$. This was much lower than the experimental value of $\sim 10^{20}\,cm^{-3}$. Thus, under commonly adopted experimental growth conditions, native point defects are unlikely to be responsible for the high hole concentrations measured in this spinel. However, *p*-type behavior is observed because holes are majority carriers. Unintentional impurities and their related defect complexes may be sources of the high hole concentrations that have been measured. Identifying those defects may lead to enhanced *p*-type $ZnRh_2O_4$ doping.

SUPPLEMENTARY MATERIAL

See the supplementary material for a table that describes the atomic relaxation of native defects in the neutral charge state.

ACKNOWLEDGMENTS

This work was supported by the Graduate School of Kasetsart University, Kasetsart University Research and Development Institute (KURDI). We thank A. Janotti for fruitful discussions. A.B. was supported by the Institute for Promotion of Science and Technology (DPST Research Grant No. 009/2558) and thanks S. Jungthawan for his advice. We wish to thank the high-performance computing facilities at the Synchrotron Light Research Institute (SLRI, Thailand) and King Mongkut's University of Technology Thonburi (KMUTT, Thailand) for their hospitality.

REFERENCES

[1]P. Manivannan and A. Subrahmanyam, J. Phys. D Appl. Phys. **26**, 1510 (1993).
[2]P. P. Edwards, A. Porch, M. O. Jones, D. V. Morgan, and R. M. Perks, Dalton Trans. **0**, 2995 (2004).
[3]W. Cui, X. Zhao, Y. An, D. Guo, X. Qing, Z. Wu, P. Li, L. Li, C. Cui, and W. Tang, J. Phys. D Appl. Phys. **50**, 135109 (2017).
[4]T. Minami, Thin Solid Films **516**, 5822 (2008).
[5]B. G. Lewis and D. C. Paine, MRS Bull. **25**, 22 (2000).
[6]T. Kamiya and H. Hosono, Int. J. Appl. Ceram. Technol. **2**, 285 (2005).
[7]G. García-Alvarado, F. de Moure-Flores, S. Mayén-Hernández, D. Santos-Cruz, E. Rivera-Muñoz, G. Contreras-Puente, M. Pal, and J. Santos-Cruz, Vacuum **142**, 175 (2017).
[8]K. G. Wilson, Rev. Mod. Phys. **47**, 773 (1975).
[9]R. Bulla, N.-H. Tong, and M. Vojta, Phys. Rev. Lett. **91**, 170601 (2003).
[10]R. Bulla, H.-J. Lee, N.-H. Tong, and M. Vojta, Phys. Rev. B **71**, 045122 (2005).
[11]R. Bulla, T. A. Costi, and T. Pruschke, Rev. Mod. Phys. **80**, 395 (2008).
[12]H. Kawazoe, H. Yanagi, K. Ueda, and H. Hosono, MRS Bull. **25**, 28 (2000).
[13]P. A. Cox, *Transition Metal Oxides: An Introduction to Their Electronic Structure and Properties* (Clarendon, Oxford, 1992).
[14]H. Mizoguchi, M. Hirano, S. Fujitsu, T. Takeuchi, K. Ueda, and H. Hosono, Appl. Phys. Lett. **80**, 1207 (2002).
[15]M. Dekkers, G. Rijnders, and D. H. Blank, Appl. Phys. Lett. **90**, 021903 (2007).
[16]N. Mansourian-Hadavi, S. Wansom, N. H. Perry, A. R. Nagaraja, T. O. Mason, L.-h. Ye, and A. J. Freeman, Phys. Rev. B **81**, 075112 (2010).
[17]A. R. Nagaraja, N. H. Perry, T. O. Mason, Y. Tang, M. Grayson, T. R. Paudel, S. Lany, and A. Zunger, J. Am. Ceram. Soc. **95**, 269 (2012).
[18]D. O. Scanlon and G. W. Watson, Phys. Chem. Chem. Phys. **13**, 9667 (2011).
[19]J. Heyd, G. E. Scuseria, and M. Ernzerhof, J. Chem. Phys. **118**, 8207 (2003).
[20]O. Volnianska and P. Boguslawski, J. Appl. Phys. **114**, 033711 (2013).
[21]O. Volnianska and P. Boguslawski, J. Phys. D Appl. Phys. **47**, 465101 (2014).
[22]A. Alkauskas, P. Broqvist, and A. Pasquarello, Phys. Rev. Lett. **101**, 046405 (2008).
[23]A. Alkauskas, P. Broqvist, and A. Pasquarello, Phys. Status Solidi B **248**, 775 (2011).
[24]A. Alkauskas and A. Pasquarello, Phys. Rev. B **84**, 125206 (2011).
[25]M. Amini, H. Dixit, R. Saniz, D. Lamoen, and B. Partoens, Phys. Chem. Chem. Phys. **16**, 2588 (2014).
[26]S. Na-Phattalung, M. F. Smith, K. Kim, M.-H. Du, S.-H. Wei, S. Zhang, and S. Limpijumnong, Phys. Rev. B **73**, 125205 (2006).
[27]P. Baranek, G. Pinarello, C. Pisani, and R. Dovesi, Phys. Chem. Chem. Phys. **2**, 3893 (2000).
[28]A. Janotti and C. G. Van de Walle, Phys. Rev. B **76**, 165202 (2007).
[29]C. Freysoldt, B. Grabowski, T. Hickel, J. Neugebauer, G. Kresse, A. Janotti, and C. G. Van de Walle, Rev. Mod. Phys. **86**, 253 (2014).
[30]P. E. Blöchl, Phys. Rev. B **50**, 17953 (1994).
[31]G. Kresse and J. Furthmüller, Phys. Rev. B **54**, 11169 (1996).
[32]K. Momma and F. Izumi, J. Appl. Crystallogr. **44**, 1272 (2011).
[33]C. Freysoldt, J. Neugebauer, and C. G. Van de Walle, Phys. Rev. Lett. **102**, 016402 (2009).
[34]P. Deák, B. Aradi, and T. Frauenheim, Phys. Rev. B **83**, 155207 (2011).
[35]A. Banerjee and Z. Singh, J. Solid State Electrochem. **13**, 1201 (2009).
[36]T. R. Paudel, S. Lany, M. d'Avezac, A. Zunger, N. H. Perry, A. R. Nagaraja, T. O. Mason, J. S. Bettinger, Y. Shi, and M. F. Toney, Phys. Rev. B **84**, 064109 (2011).
[37]P. Reunchan and N. Umezawa, Phys. Rev. B **87**, 245205 (2013).
[38]K. Reuter and M. Scheffler, Phys. Rev. B **65**, 035406 (2001).
[39]C. G. Van de Walle, Phys. Rev. B **56**, R10020 (1997).
[40]C. G. Van de Walle, Phys. Rev. Lett. **85**, 1012 (2000).